ANALYSIS OF ω CENTAURI USING APERTURE PHOTOMETRY

LUCY ARROWSMITH
30655218

Abstract

This report studies the globular cluster ω Cen, NGC 5139 using photometric methods to estimate the age, colour and distance. Utilising Girardi Isochrones to estimate the best fit against the V-I colour-magnitude diagram, and offsetting the isochrone using dust extinction $E(B-V)\sim 0.3$ and distance modulus $(m-M)\sim 13.5$, we determined the distance $d = 5.012 \pm 0.5\ kpc$ and age at approximately 10.935Gyrs. The distance calculated is consistent with Baumgardt's (2016) value within 2-sigmas of the canonical value $d = 5 \pm 0.5 kpc$ obtained from photometric methods. The best fit isochrone of 10.935Gyrs, is used to estimate the metallicity $[M/H]\sim -2$, which is found within the broad range of metallicities in ω Cen of ~ -1.7 to ~ -2.2.

1. *Introduction*:

Globular clusters are a collection of stars in a spherical formation, of which Omega Centauri (ω Cen), NGC 5139, is the largest and most luminous globular cluster in the Milky Way (Sollima et al., 2005). With an estimated mass between $2.4 \times 10^6 M_\odot$ and $5.1 \times 10^6 M_\odot$ (Mandushev et al. 1991 and Meylan et al., 1995 as cited by G. van de Ven et al., 2005 respectively) and its multiple stellar populations along the red giant and main sequence branch (Sollima et al. 2005), it has been a point of interest for many astrophysicists. Because this is atypical for a globular cluster, astrophysicists have suggested numerous formation theories such as, the remnant of a dwarf galaxy caused by a merger with the Milky Way or a merger between two globular clusters. Furthermore, due to the relatively weak gravitational pull of ω Cen, with a concentration index log(rt/rc) ∼ 1.24, it has been possible to study stars within the cluster individually (G. van de Ven et al., 2005).

This paper will aim to use aperture photometry to determine age, colour, and distance of ω Cen. For example, Solima et al. (2005) determined, using multiband colour-magnitude diagrams, that the stars are not distributed continuously. Rather, there are at least four distinct populations each with identifiable metallicity distributions. This could imply that the stellar population groups of ω Cen can be described by varying star formations.

We focus on estimating the age and metallicity through photometric methods using Girardi isochrones of fixed metallicity and varying age and vice versa (Girardi L., 2021). We will use dust extinction *E(B-V)* and distance modulus *(m-M)* as free parameters to be obtained from fitting isochrones to BVRI colour-magnitude diagrams.

2. *Method*:

On the 28th of March 2020, we observed ω Cen at Monash University's Hutton-Westfold Observatory. Using the C11 telescope, we captured bias, dark, flat-field and science images. However, due to high cloud coverage over the flat-field frames on the 28th of March, we proceeded to use flat-field images from the 29th of March. The science images of ω Cen were captured using *BVRI* filters at 30 second exposures.

2.1. Processing and combining images.

To process the science images, in Python3 we used Astropy scripts ccdproc and CCDData to reduce and read the files. Once we obtained a combined median bias image, we ensured the dark frames had a CCD temperature at approximately -20°C and subtracted the median bias from each image in the dark frames. These reduced bias and dark frames were then subtracted from each *BVRI* band flat-field images and combined. The median combined images are used to correct for dust doughnuts, vignetting, non-uniform light distribution and hot pixels from the raw science images.

The stellar positioning in each frame is corrected and shifted using a reference star to offset each *BVRI* band against its respective reference star. We fitted 1D and 2D Gaussians over a centroid of the reference star to determine the pixel coordinates and offset these images to the reference image, hence aligning the stellar positioning. We confirmed the image had aligned correctly using SAOImageDS9, neglecting any image with high cloud coverage that generated poorly shifted images.

Next, we determined the flux of a 20pixel radius aperture over multiple bright stars and generated a medium value of aperture sums per frame, converting to units of ADU. We used two methods to determine the combined images, median and average, and write these to the respective FITS files.

2.2. Generating catalogues and calibrating images

We generated a multi-dimensional array of magnitudes from Graham 1982 Standard stars text file. We chose a bright reference star, within radius of 725pixels from ω Cen's centre, at coordinates $\alpha = 201°52153221085$ and $\delta = -47°39518238257$ and generated the *G, G_{BP}* and *G_{RP}* magnitudes. Next, we used the following set of equations that relate *GAIA* to *BVRI* magnitudes provided by [Monash Reference],

$$
\begin{aligned}
B &= -0.03308 + 1.41139 * G_{BP} + G_{BP} \\
V &= 0.00858 + 0.22184 * (G_{BP} - G) + 0.48446 * (G_{BP} - G)^2 + G \\
R &= 0.01283 + 0.33460 * (G - G_{RP}) + 0.40048 * (G - G_{RP})^2 + G_{RP} \\
I &= 0.00216 - 0.14069 * (G - G_{RP}) + G_{RP}.
\end{aligned}
\qquad \text{- (1)}
$$

Where *B, V, R and I are the magnitudes and* G_{BP}, G and G_{RP} are the GAIA magnitudes determined from the reference star.

We generated a catalogue of stars for each average and median combined *BVRI* images and applied circular aperture photometry at a pixel radius of 10 pixels. We found the V-band filter to have the deepest catalogue of stars and used the *V*-band aperture positions as a reference to use in the *BRI*-band images. Next, we created a photometry table of aperture pixel coordinates and their respective aperture sum. Similarly, a photometry table was generated for each band and using the reference star, we offset the aperture positions to align with the *V*-band. This ensures each aperture surrounding a star has the corrected pixel coordinates and appropriate aperture sum in the respective *BVRI* photometry table. We use these adjusted photometry tables to determine the *BVRI* fluxes for the reference star.

2.3. Magnitudes

With the chosen reference stars and the *BVRI* fluxes, we used the generic formula Eq. (2) to obtain an array of apparent magnitudes in the *BVRI* filters,

$$m_V = 2.5 \log_{10}\left(\frac{VRefFlux}{f_{i,V}}\right) + V. \qquad \text{- (2)}$$

Where m_v is the apparent magnitude for the *V*-band, *VRefFlux* is the flux of the reference star in *V-band*, $f_{i,V}$ is the aperture sum for each star in *V*-band photometry table and V is the magnitude determined from Eq.(1). We use variations of Eq. (2), to the respective band filters.

2.4. Girardi Isochrones and HR Diagrams

We generated Hertzprung-Russell (HR) Diagrams for *V*-band apparent magnitudes as a functions of *B-V, V-I, R-I* and *V-R*. We included both average and the median combined plots to determine which method best fits the globular cluster. To decrease the possibility of artificially saturated stars mixed with the data, we excluded all stars in the *V*-band with peak counts greater than 60,000.

From Girardi L. (2021), we generated isochrones at ages beginning from 640Myrs to 16.402Gyrs. We fitted the isochrones against the HR diagrams and offset the plots by estimating the dust extinction *E(B-V)* values at 0.28 to 0.3, and the distance modulus *(m – M)* at 13 to 13.5, until the isochrones were well fitted against the data. We utilise E(B-V) to offset the isochrone in the vertical and 3.1*E(B-V) in the horizontal,

Lastly, we generated the best fit isochrone age of 10.935Gyrs for the *V*-band apparent magnitude as a function of *V-I*, with metallicity $[M/H] = -0.5\ to\ -2.7$ and plotted these against the *V-I* HR scatter diagram. Using the offset values for the distance modulus *(m-M)* we calculated the distance to ω Cen using Eq. (3) where *d* is the distance in parsecs,

$$d = 10 * 10^{0.2(m-M)}. \qquad \text{-(3)}$$

3. Results and Analysis:

We briefly discussed in the method the process of correctly combining and scaling the images to obtain a median and average combined FITS image. For this report, we will be using the median combined image as our primary source of analysis. We found a large increase in hot pixels in the median average image compared to the median combined, which increased the average flux over the apertures.

The reference star at $\alpha = 201°52153221085$ and $\delta = -47°39518238257$ generated the following magnitudes: $G = 11.111 \pm 0.067$, $G_{BP} = 10.830 \pm 0.022$ and $G_{RP} = 10.156 \pm 0.051$. Using Eq. (1), the GAIA magnitudes produced the following results in Table 1.

Filter	Pixel Coordinates (x,y)	Magnitude	Flux (ADUs)
B	(1372.77, 169.75)	11.475	48236 +- 219
V	(1383.89, 167.98)	10.939	227280 +- 477
R	(1396.07, 165.72)	10.576	162133 +- 403
I	(1358.80, 177.74)	10.063	176037 +- 419

***Table 1**: BVRI magnitudes of the reference star at $\alpha = 201°521$ and $\delta = -47°395$ and their respective fluxes*

Whilst processing the images, we found the *V*-band median image to have the highest visibility with 3025 stars observed, while the *B*-band median image observed 2011 stars. We noted on the observation night of 28th

March, the cloud coverage was high at approximately 30% over the *B*-band exposures. Hence, the resulting flux of 48236 ADUs is expected for the *B*-band in Table 1.

We generated photometry tables for *BVRI* bands and assigned *V*-band aperture positions to each *BRI* image. As shown in Figure 1, we used photometric calibration and aperture photometry of 10-pixel radii in the *V*-band. We see the dense population of stars organised in the centre, where many stars have not been identified by the apertures.

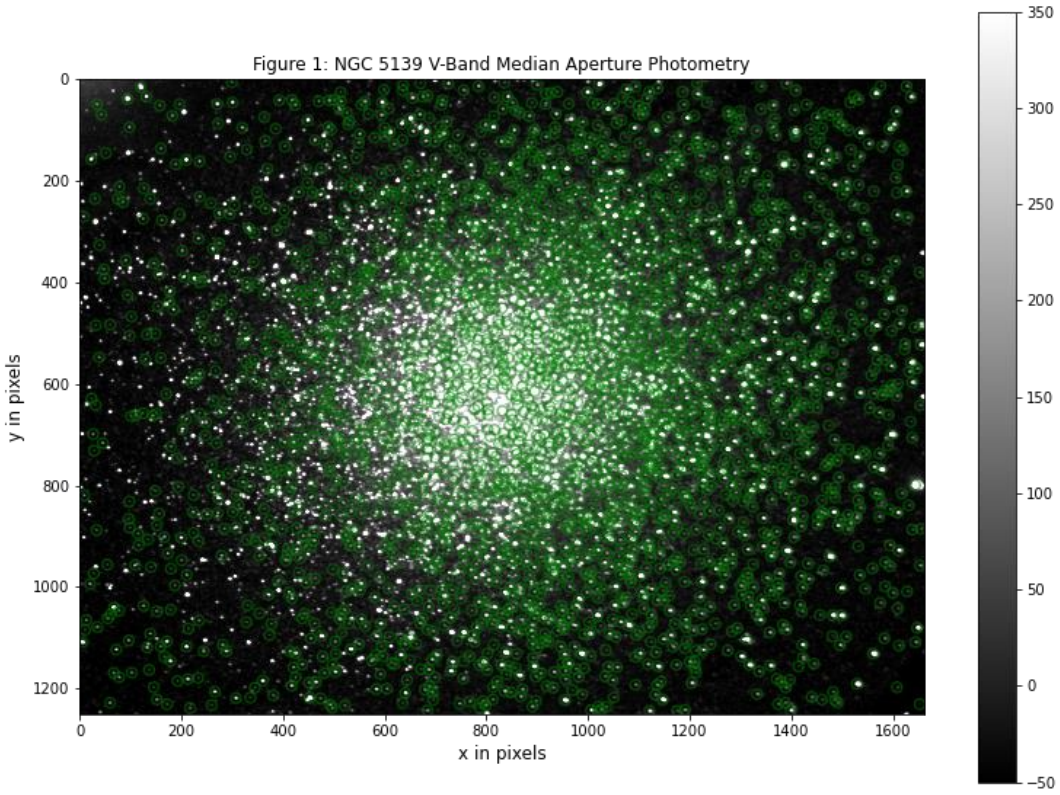

Figure 1: *Aperture V-band photometry of 3025 stars in NGC 5139, with a radius of 10pixel per aperture.*

We present the comparison between the colour magnitude HR diagrams against the apparent magnitude in figure 2 below.

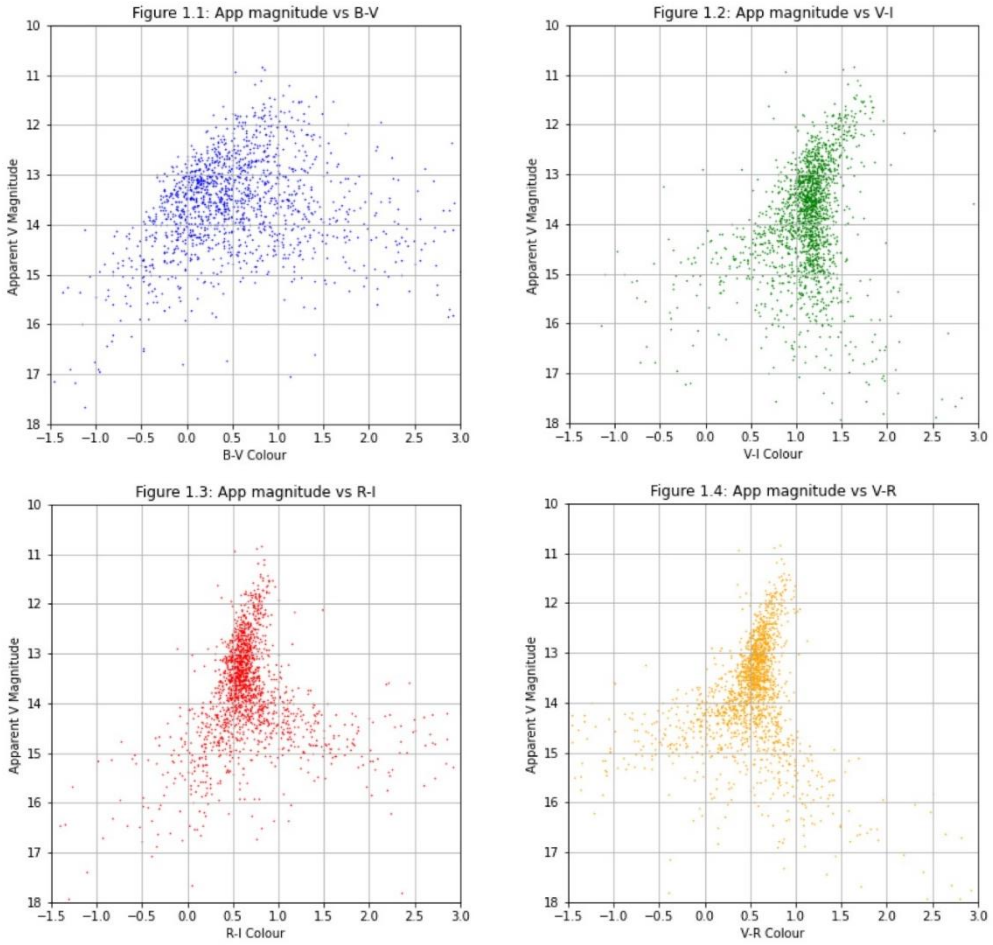

Figure 2: *Colour-magnitude diagrams of B-V, V-I, R-I and V-R. The relation for dust reddening is E(B-V) =0.3 and the distance modulus (m-M) =13.5.*

As shown above, *B-V* colour magnitude diagram has a distinct lack of structure and will not be used in the analysis for this report. This could be the result of high cloud coverage over all images, resulting in a lower number of stars calibrated and aperture sums dimmer than comparative *VRI* bands. In comparison to appendix 2, the colour is bluer at an average of $B-V \sim 0.6$ at $V \sim 19$, whereas figure 1.1 has an average colour of $B-V \sim 0.2$ at $V \sim 14$.

The Red Giant Branch (RGB) can be seen in all figure 2 images in the upper right, extending off from the Main Sequence (MS) turn off at approximately 14 and 15 magnitudes. Assuming the stars are of solar abundance, the stars of $V > 15$ are at the end of the MS branch and stars $V < 15$ are a member of the RGB. At the MS turn off, there is a large proportion of stars that have colours $V-I < 0.5$, $R-I < 0.2$ and $V-R < 0.2$, possibly indicating these stars are blue stragglers or noise.

We used the Girardi Isochrones generated at varying ages and plotted these against the *V-I* colour-magnitude diagram in figure 3. Applying distance modulus offset $(m-M) = 10.5$ and dust extinction $E(B-V) = 0.15$, shifted the isochrones to align with the *V-I* structure. The distance derived using $E(B-V) \sim 0.15$ and $(m-M) = 10.5$ was $d = 1.259 \pm 1\ kpc$.

We determined age 10.935Gyr fitted relatively well between 1-sigma scatter of ~ 0.1mags to the *V-I* colour-magnitude diagram as seen in figure 3, using this isochrone as our estimated age for ω Cen.

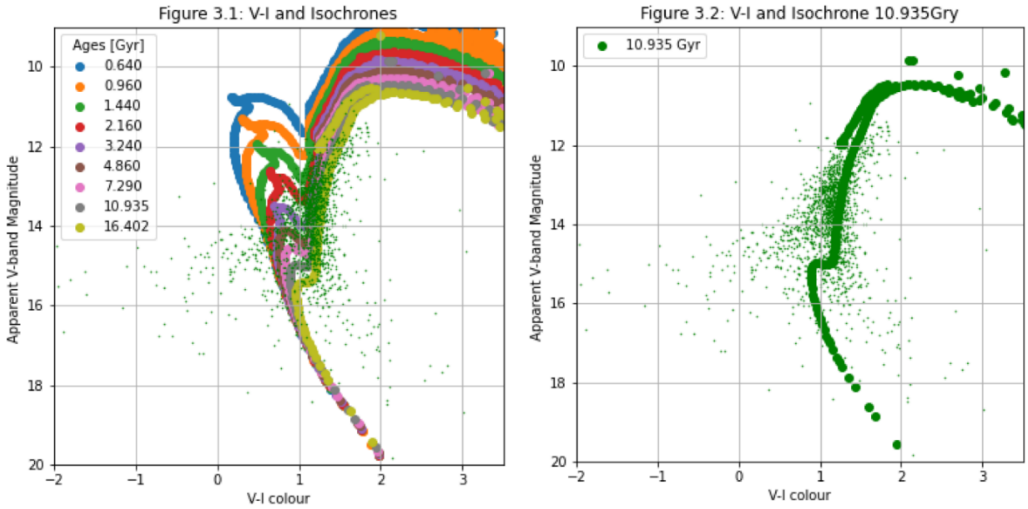

Figure 3: *V-I colour-magnitude against varying ages of isochrones from 640Mys to 16.402Gyrs. Figure 3.2 illustrates age 10.935Gyrs best-fit the data with E(B-V)~0.15 and (m-M)~10.5.*

These are not the expected values indicated by Sollima, Ferraro et al., 2005. We therefore generated an isochrone fixed at the age of 10.935Gyrs, with a metal to hydrogen ratio $[M/H]$ between $-0.5\ to\ -2.7$ and plot these against *V-I* colour-magnitude diagram. We see in figure 4 at 10.935Gyrs, that metallicities from $[M/H]\sim -2.3$ and below are the best fit. Comparing the metallicity fits, we observed $[M/H]\sim -2$ aligns best with the data.

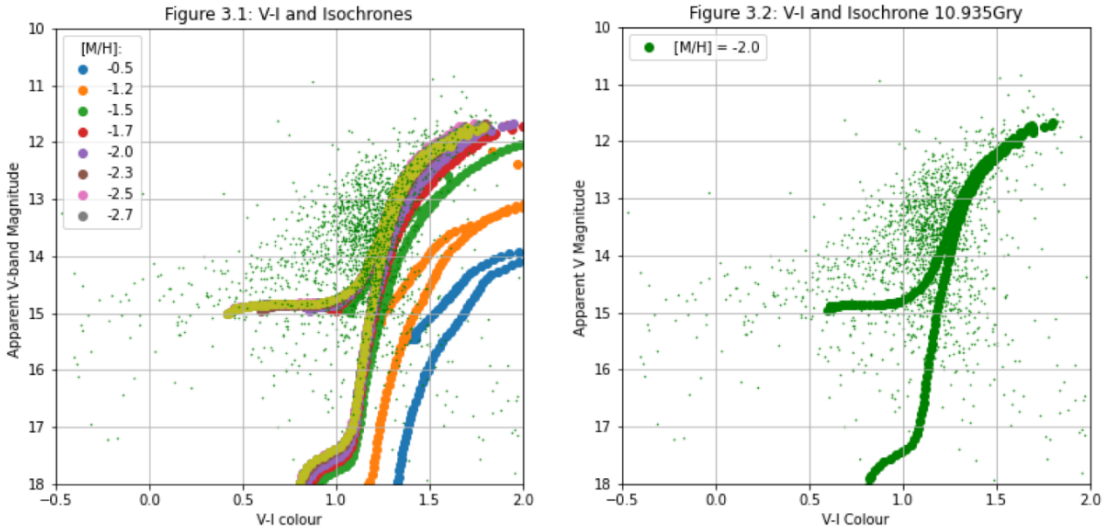

Figure 4: *Isochrone of age 10.935Gyrs with a range of metallicities in Figure 3.1. Figure 3.2 illustrates [M/H]=-2.0 fits the data well.*

Using Eq.(3), we calculated the distance to ω Cen using the offset values of $(m-M)\sim 13.5$, and determined the distance as $d = 5.012 \pm 0.5\ kpc$.

4. Discussion:

The investigation of distance using multiple ages at a set metal fraction Z=0.0152, found our parameters $E(B-V)\sim 0.15$ and $(m-M)\sim 10.5$ to be underestimated in comparison to $E(B-V) = 0.3$ and $(m-M) = 13.75 \pm 0.13$ (Sollima, Ferraro et al., 2005). Using these resulted in a distance $d = 1.259 \pm 1\ kpc$ and an age of 10.935Gyrs, which is greater than 6-sigma of Baumgardt's (2016) value of $d = 5 \pm 0.5 kpc$. The difference in distance indicated my assumption that ω Cen's population has a homogeneous solar abundance is not correct.

We found by changing the metallicity at the set age of 10.935Gyr, the isochrone fits relatively well between $[M/H] = -2.3$ to -2. This is not unusual due to the wide range of spectral classes within the globular cluster. We see in appendix 1, ω Cen has a range of metallicities from $[Fe/H]\sim -2.2$ to -0.5. These values agree with our estimated metallicities within $\pm$ 0.3 of the literature metal fractions.

We are not concerned about the differences in metal fractions due to the inhomogeneity of chemical abundance (G. van de Ven et al., 2005). As stated by Weldrake et al., 2007, it is not unusual for a globular cluster of ω Cen's size, with its diverse population and its metallicities to range between $[Fe/H]\sim -2.2$ to -0.5 and a peak at $[M/H]\sim -1.7$ (Johnson and Pilachowski, 2010). Comparatively, the isochrone in figure 4.2 agrees with the lower bound of Weldrake et al., 2007. The inhomogeneity of chemical abundance is one of the factors that contributes to the complicated history of ω Cen which scientists are still studying.

Using the corrected values for metallicity at $[M/H]\sim -2$ and age 10.935Gyrs, we shifted the free parameters to obtain figure 3.2. The corrected dust extinction of $E(B-V)\sim 0.3$ are in perfect agreement, whereas the distance modulus $(m-M)\sim 13.5$ is within 2-sigmas of Sollima, Ferraro et al. (2005) values mentioned above. With the corrected distance modulus, we calculated a distance of $d = 5.012 \pm 0.5\ kpc$ which is within 1-sigma of Baumgardt's (2016) distance $d = 5.0 \pm 0.5\ kpc$, calculated using photometric methods.

As mentioned by G. van de Ven et al. (2000), the evolution of ω Cen has been of great interest among astronomers and astrophysicists for decades due to the atypical observations relative to the other 200 globular clusters found in the Milky Way. One theory states it has an alternate origin to the typical globular cluster due its high mass, flattened shape, and high rotational velocity. This has caused speculation that it is a core remnant of a dwarf galaxy that was disturbed due to the collision with the Milky Way. (G. van de Ven et al., 2005).

We used the photometric method to analyse ω Cen and obtained results within 2-sigmas of the expected values as mentioned above. However, during the processing and combining of the images, we found the images in *BVRI* bands varied with visibility and other obstructions such as elongated stars caused by a disturbance to the telescope. We decided to discard these poor-quality images, resulting in a mixed number of images per filter prior to combining, hence some data may be lost in the process.

Additionally, we found approximately 700 saturated stars at peak flux greater than 60,000 counts per aperture in the *VRI*-bands and 4 in the *B*-band. These were included in the analysis and generation of the colour-magnitude diagrams. When including the saturated stars, which may have been artificially bluer, we found no difference in the fitting of age and metallicity isochrones.

5. *Conclusion*

We analysed ω Cen using aperture photometry in *BVRI*-bands and fitted Girardi isochrones at fixed age and at fixed metallicity to estimate the age, distance, and metallicity. With dust extinction values of $E(B-V)\sim 0.3$ and distance modulus of $(m-M)\sim 13.5$, we calculated the distance $d = 5.012 \pm 0.5\ kpc$. We estimated the age assuming solar abundance at Z=0.0152 and found 10.935Gyrs best-fit the V-I colour-magnitude data. This fixed age isochrone was then used to estimate the metallicity values and we determined $[M/H]$ best fits between -2 and -2.3. The distance had a 2-sigma agreement with Baumgardt's (2016) value $d = 5 \pm 0.5 kpc$.

6. References:

Sollima, A., Ferraro, F., Pancino, E. and Bellazzini, M., 2005. On the discrete nature of the red giant branch of ω Centauri. *Monthly Notices of the Royal Astronomical Society*, 357(1), pp.265-274.

Ramírez, I., Michel, R., Sefako, R., Tucci Maia, M., Schuster, W., van Wyk, F., Meléndez, J., Casagrande, L. and Castilho, B., 2012. THEUBV(RI)CCOLORS OF THE SUN. *The Astrophysical Journal*, 752(1), p.5.

G. van de Ven, van den Bosch, R., Verolme, E. and de Zeeuw, P., 2005. The dynamical distance and intrinsic structure of the globular cluster ωCentauri. *Astronomy & Astrophysics*, 445(2), pp.513-543.

Sollima, A., Ferraro, F., Pancino, E. and Bellazzini, M., 2005. On the discrete nature of the red giant branch of ω Centauri. *Monthly Notices of the Royal Astronomical Society*, 357(1), pp.265-274

Villanova, S., Geisler, D., Gratton, R. and Cassisi, S., 2014. THE METALLICITY SPREAD AND THE AGE-METALLICITY RELATION OF ω CENTAURI. *The Astrophysical Journal*, 791(2), p.107.

Mso.anu.edu.au. 2007. *Blue Straggler Stars*. [online] Available at: <http://www.mso.anu.edu.au/~jerjen/researchprojects/bluestraggler/bluestraggler.html> [Accessed 27 May 2021].

Aladin.u-strasbg.fr. 2000. *Aladin Sky Atlas*. [online] Available at: <https://aladin.u-strasbg.fr/AladinLite/> [Accessed 27 May 2021].

Jalali, B., Baumgardt, H., Kissler-Patig, M., Gebhardt, K., Noyola, E., Lützgendorf, N. and de Zeeuw, P., 2012. A DynamicalN-body model for the central region ofωCentauri. *Astronomy & Astrophysics*, 538, p.A19.

Williams, D., 2018. *Sun Fact Sheet*. [online] Nssdc.gsfc.nasa.gov. Available at: <https://nssdc.gsfc.nasa.gov/planetary/factsheet/sunfact.html> [Accessed 27 May 2021].

Baumgardt, H., 2016. N-body modelling of globular clusters: masses, mass-to-light ratios and intermediate-mass black holes. *Monthly Notices of the Royal Astronomical Society*, 464(2), pp.2174-2202.

Weldrake, D., Sackett, P. and Bridges, T., 2007. A Deep Wide-Field Variable Star Catalog of ω Centauri. *The Astronomical Journal*, 133(4), pp.1447-1469.

Johnson, C. and Pilachowski, C., 2010. CHEMICAL ABUNDANCES FOR 855 GIANTS IN THE GLOBULAR CLUSTER OMEGA CENTAURI (NGC 5139). *The Astrophysical Journal*, 722(2), pp.1373-1410.

Monash University ASP3231, *GAIA – BVRI photometry relations*

Girardi, L., 2018. *CMD 3.4 input form*. [online] Stev.oapd.inaf.it. Available at: <http://stev.oapd.inaf.it/cmd> [Accessed 30 May 2021].

7. Appendices:

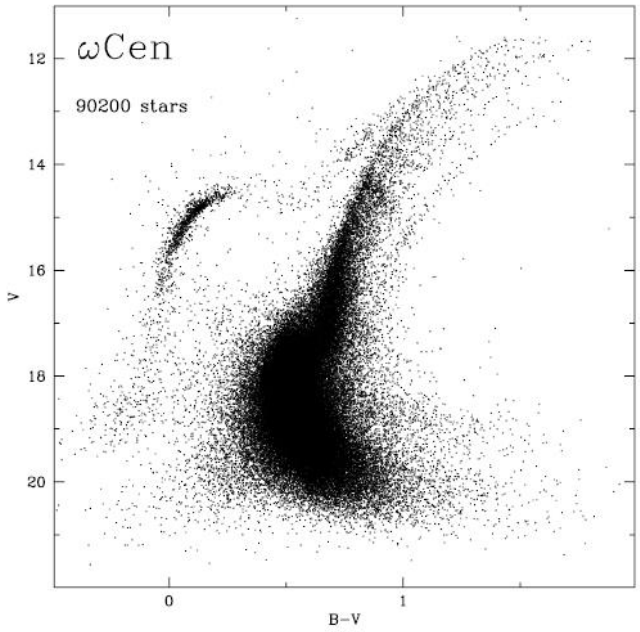

Appendix 1: *(V, B-V) CMD for the globular sample of ~90 000 stars measured in Ω Cen. (*Sollima, Ferraro et al., 2005)

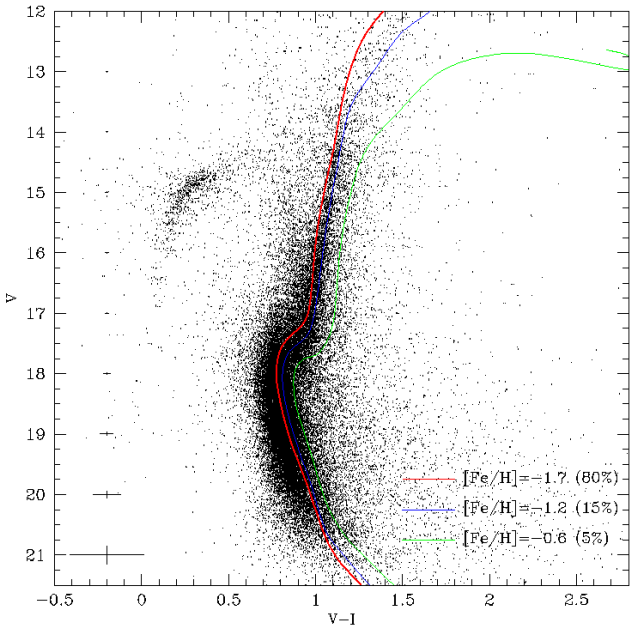

Appendix 2: *(V, V-I) CMD for Ω Cen with three theoretical isochrones to define the stellar populations of the cluster.* (Yi et al., 2003 and Norris et al., 2004 as cited by Weldrake, et al., 2007)